行政院國家科學委員會專題研究計畫　成果報告

總計畫(I)

計畫類別：整合型計畫
計畫編號：NSC93-2218-E-009-015-
執行期間：93 年 08 月 01 日至 94 年 07 月 31 日
執行單位：國立交通大學電信工程學系(所)

計畫主持人：蘇育德
共同主持人：楊谷章，翁芳標

報告類型：精簡報告

處理方式：本計畫可公開查詢

中　華　民　國 94 年 10 月 28 日

行政院國家科學委員會專題研究計畫成果報告

下一世代無線行動接取技術-總計畫

Next Generation Mobile Radio Access Technologies (I)

計畫編號：NSC 93-2218-E-009-015
執行期限：93 年 8 月 1 日至 94 年 7 月 31 日
主 持 人：蘇育德 交通大學電信工程學系

中文摘要

在第三代的通訊系統技術的標準制定完成，而且也逐漸進入商業化的程序之後，無論是學界或工業界都已開始在思索著下一代的通訊系統 (Beyond Third Generation, B3G)的可能架構與技術。新一代的通訊系統(B3G)預期將提供更全面性的服務，包括高速的資料傳輸、多媒體服務及數據行動通訊，使無線通訊的產業更加蓬勃。

每個新一代無線通訊系統從觀念的孕育到標準的制訂完成通常需要十年以上的時間。關於下一代的無線通訊系統(Beyond Third Generation, B3G)的演進，按 ITU-R 的初步藍圖，其時程將綿延近二十年。因此，在 3G 已有初步小規模的佈建之際，國際上已成立了世界無線研究論壇(Wireless World Research Forum, WWRF)，集結了各國（以歐盟為主）產、學界的尖端研發人才，開始研究新一代無線通訊系統的架構。

下一代的無線通訊系統預期將提供更全面性的服務，包括高速的資料傳輸、無線多媒體服務及數據行動通訊。雖然我們無法預期下一代的通訊系統的完整架構，但是我們可以確定的是 B3G 無線通訊系統的設計核心仍是在新的傳輸介面(Air Interface)，即無線接取技術(Wireless Access Technology)之確立。本計劃為三年期計劃的第一年，我們提出一完整的無線接取架構，並透過分析、模擬證明其可行性。

本總計畫含括三個子計劃，計劃名稱分別為：

(1) 下一世代無線行動接取技術 - 子計劃一:多通道多速率展頻技術。
(2) 下一世代無線行動接取技術 - 子計畫三:時空信號處理及多用戶檢測。
(3) 下一世代無線行動接取技術 - 子計劃四:同步、通道估計與內接收機設計。

各個子計劃所發展的成果將在本報告中以獨立章節做一重點性的說明，並輔以軟體模擬成果以提供完整的系統性能評估之用。

關鍵詞：無線通訊，行動無線接取技術，B3G。

Abstract

Although the deployment of the 3G systems had met some difficulty and the debate on the future perspective of the 3G systems results in no definite conclusion. Research institutes, major equipment providers as well as operators from all over the world had joined forces to look into future generations (beyond the third generation, B3G) of wireless communications, creating the Wireless

World Research Forum (WWRF).

It is expected that the air interface will be playing the central role of the B3G wireless network. In this report, we propose a new broadband wireless mobile access architecture that is suitable for high-speed multimedia wireless transmission, predict its overall performance, and validate its feasibility. We produce simulation programs so that future users can emulate the performance of our joint design. This joint effort consists of tree sub-projects, namely,

1. Multi-channel multi-rate spreading sequences technologies.
3. Space-time signals processing and multi-user detection.
4. Synchronization, channel estimation and inner receiver design.

It is clear that each sub-project studies a vital part of a broadband wireless mobile transmission system and all of them are closely coupled. For detailed description of each sub-project please refer to the sub-project reports.

Keywords: Wireless Communication, Mobile Radio Access Technologies, B3G.

1. Introduction

下一代新的無線接取技術到底為何，是繼續發展、改善 3G 的 CDMA 技術或需要新的接取技術，雖然以歐、日大廠的研發趨勢與成果來判斷後者的可能性較高，但現在尚無法確定。就目前的資料來看，基本的傳輸要求至少包括了：

(1). 低速環境傳輸率 > 155 Mbps
(2). 低速環境傳輸率 > 2 Mbps
(3). 系統容量 > 10 倍 3G 容量

要達到這個目標當然得要改善3G的傳輸技術。本計畫所從事研究之接取技術，係為目前無線寬頻通訊產、學業中積極發展，頗具潛力的研究課題，也是未來B3G無線通訊系統運用所需建立的關鍵技術。我們研發的成果，累積的技術能量可提供業界諮詢，所培訓人員更可給予國內通訊產業運用。除此之外，本計畫所研究具備高效率、高彈性、高適應性的系統架構，可供完整的系統性能模擬、評估之用。

我們這個計畫分為三個子計畫，將分別就這些發展中技術做深入的研究。三個子計畫的名稱與主持人為：

一、下一世代無線行動接取技術：多通道多速率展頻技術（中興大學 楊谷章教授）
二、下一世代無線行動接取技術：時空信號處理及多用戶檢測（中興大學 翁芳標助理教授）
三、下一世代無線行動接取技術: 同步、通道估計與內接收機設計（交通大學 蘇育德教授）

以上三個子計畫在整個傳輸介面所探討的部分及互相之整合程度請參見各子計畫計畫書。綜合言之，各子計畫負責傳輸介面的一特定環節，互補性與相關性至為明顯，缺一不可。基本上，我們是以可調式多天線、多傳輸率的 OFDM/CDMA 系統為基礎架構。我們的研究成果除了可運用於 B3G 的行動通訊外，也旁及無線區域網路如 IEEE 802.11a、g，個人區域網路(Wireless Personal Area Network, WPAN)及廣域網路如 IEEE 802.16 等之應用。

在下列章節中，我們將就各子計劃內容做一重點性說明。

2. 下一世代無線行動接取技術-子計劃一：多通道多速率展頻技術

2.1 Introduction

In order to support higher data transmission rates and more multimedia applications than the present 2G systems, multicarrier direct-sequence code- division multiple access (MC/DS-CDMA) techniques have been proposed and applied widely for wireless communication, such as in beyond 3G systems [1.1][1.4]. MC/DS-CDMA schemes have several advantages, including narrowband interference suppression, multipath fading robustness, and lower chip rate than single-carrier systems occupying the same total bandwidth [1.5], [1.6]. In the MC/DS-CDMA systems, the system performance gets worse as multiple- access interference (MAI) increases. Therefore, interference rejections by the use of some special spreading codes are important issues in the new generation systems. As compared with the orthogonal variable spreading factor (OVSF) codes [1.7], [1.8], 2-D OVSF codes can eliminate MAI in asynchronous MC/DS-CDMA and get higher bandwidth efficiency.

2.2 2-D OVSF Codes

A class of 2-D OVSF codes was proposed in [1.9] to eliminate MAI by providing mutual orthogonality among code matrices and improve the capacity and throughput of multiple-rate, multimedia MC/DS-CDMA systems. In addition, our 2-D OVSF codes have the advantage of being conveniently generated in a tree structure and maintaining orthogonality in the code tree.

Each 2-D spreading code sequence is a binary (+1,-1) bipolar $M \times N$ matrix, where M is the number of rows, related to the number of available frequency carriers, and N is the number of columns, related to the code length. In [1.9], new constructions provide the 2-D spreading codes with $M=2^k$ and $N=2^l$, where k and l are positive integers, and $k \le l$. In IMT-2000 with W-CDMA, 1-D OVSF codes provide the foundation for supporting multi-rate data services. Similarly, the proposed 2-D orthogonal also offers the variable-length spreading and multicode capacities. In addition, the new 2-D OVSF codes possess zero cyclic auto- and cross-correlation properties.

A. Construction of $\mathrm{A}_{2^k \times 2^k}^{(i)}$

Let $N=2^k$ and k be a positive integer. The generation of the first 2-D OVSF code with matrices $\mathrm{A}_{N\times N}^{(i)}$ (for $i \in \{1,2,...,N\}$) of size $N \times N$, length N, and cardinality N starts with k=1, which involves two orthogonal matrices

$$\mathrm{A}_{2\times 2}^{(1)} = \begin{bmatrix} + & + \\ + & - \end{bmatrix}, \quad \mathrm{A}_{2\times 2}^{(2)} = \begin{bmatrix} + & - \\ + & + \end{bmatrix}$$

where "+" represents "+1" and "–" denotes "-1". The procedure continues with $N=2^2$ (i.e., k=2) in accordance to

$$\mathrm{A}_{4\times 4}^{(1)} = \left[\mathrm{A}_{2\times 2}^{(1)} \otimes \mathrm{A}_{2\times 2}^{(1)}\right] = \begin{bmatrix} + & + & + & + \\ + & - & + & - \\ + & + & - & - \\ + & - & - & + \end{bmatrix}$$

$$\mathrm{A}_{4\times 4}^{(2)} = \left[\mathrm{A}_{2\times 2}^{(2)} \otimes \mathrm{A}_{2\times 2}^{(1)}\right] = \begin{bmatrix} + & + & - & - \\ + & - & - & + \\ + & + & + & + \\ + & - & + & - \end{bmatrix}$$

$$\mathrm{A}_{4\times 4}^{(3)} = \left[\mathrm{A}_{2\times 2}^{(1)} \otimes \mathrm{A}_{2\times 2}^{(2)}\right] = \begin{bmatrix} + & - & + & - \\ + & + & + & + \\ + & - & - & + \\ + & + & - & + \end{bmatrix}$$

$$\mathrm{A}_{4\times 4}^{(4)} = \left[\mathrm{A}_{2\times 2}^{(2)} \otimes \mathrm{A}_{2\times 2}^{(2)}\right] = \begin{bmatrix} + & - & - & + \\ + & + & - & - \\ + & - & + & - \\ + & + & + & + \end{bmatrix}$$

where $\otimes$ denotes the Kronecker product of two matrices. In general, with $k > 1$, our first 2-D OVSF codes of size $N \times N$, length N, and cardinality N=2^k can be constructed by the recursive procedure.

B. Construction of $A^{(i)}_{2^k \times 2^{k+\alpha}}$ *with* $\alpha \geq 1$

Let $M=2^k$, $N=2^{k+\alpha}$, and k and α be positive integers. The generation of the second 2-D OVSF codes with matrices $A^{(i)}_{M \times N}$ (for $i \in \{1, 2, ..., M\}$) of size $M \times N$, length N, and cardinality M starts with $k=1$, such that

$$A^{(1)}_{2\times 4} = \begin{bmatrix} A^{(1)}_{2\times 2} & A^{(2)}_{2\times 2} \end{bmatrix} \begin{bmatrix} + & + & + & - \\ + & - & + & + \end{bmatrix},$$

$$A^{(2)}_{2\times 4} = \begin{bmatrix} A^{(1)}_{2\times 2} & -A^{(2)}_{2\times 2} \end{bmatrix} \begin{bmatrix} + & + & - & + \\ + & - & - & - \end{bmatrix}$$

The procedure continues with $M=2^1$ and $N=2^{1+\alpha}$ for a given $\alpha \geq 1$ in accordance to

$$A^{(1)}_{2\times 2^{1+\alpha}} = \begin{bmatrix} A^{(1)}_{2\times 2^{\alpha}} & A^{(2)}_{2\times 2^{\alpha}} \end{bmatrix},$$

$$A^{(2)}_{2\times 2^{1+\alpha}} = \begin{bmatrix} A^{(1)}_{2\times 2^{\alpha}} & -A^{(2)}_{2\times 2^{\alpha}} \end{bmatrix}.$$

For M and N with arbitrary powers of 2, the code matrices with various code lengths and the number of available carriers can be constructed by using a tree structure with various $\alpha \geq 0$. Any two 2-D OVSF matrices in the same layer (and with the same α in the second construction) are orthogonal. Furthermore, any two matrices in different layers but with the same α are also orthogonal, except that one of them is a mother matrix of the other. Therefore, the number of available matrices can be used by other users depends not only on the total number of matrices in the code tree but also the number of mother and child matrices of those already assigned matrices.

2.3 System Model

For the kth user, the random binary data bit stream is multiplied by the code sequence $C_{k,j}(t)$ (for $j \in [1, M]$), and is transmitted by the jth carrier w_j in the jth frequency band, where $C_{k,j}(t)$ represents the jth row of the distinct 2-D OVSF code matrix designated to user k.

The receiver of the kth user is given in the report of sub-project 1, in which an M-branch bandpass filter/diversity combiner RAKE receiver is used. The MC/DS-CDMA signals detected at the receiver are first frequency-filtered into M diversity branches in according to the signals' carriers. The M filtered and despread signals, Z_j (for $j \in [1, M]$), from a decision sample per bit period are individually weighted and then combined by a combiner. Two diversity combining methods which are commonly used in the RAKE receiver, maximum-ratio combing (MRC) and equal-gain combing (EGC) are considered in this project.

In this project, we consider three channel models, that is, AWGN non-fading channel, Rayleigh fading channel and Rician fading channel to provide the performance analysis. In an AWGN non-fading channel, we assume that the received signal has complete carrier-phase coherency and non-fading amplitude. In a Rayleigh fading channel, the phase and fading amplitude of the received signal is uniformly distributed and Rayleigh distributed, respectively. However, the fading effects on phase and amplitude can often severely degrade system performance. The Rician channel is a kind of weak fading channels, in which the fading amplitude follows a given Rician parameter R, as described in [1.10]. In other words, as compared with a Rayleigh fading channel, the fading effects which the received signal experiences in a Rician fading channel is relative small.

2.4 Performance Analysis

A. Error probability under an AWGN non-fading channel

In an AWGN non-fading channel, the performance of the multicarrier system using 1-D Gold codes is poorer than that of using 2-D OVSF codes. This is because, in such AWGN non-fading channel, the frequency diversity is relative small but the system using the 1-D Gold codes has no code diversity in each carrier branch. If we have larger

number of hits in 1th sub-channel, the following *M*-1 sub-channels will suffer the same number of hits. This makes the interference caused by the specular terms of the received signal almost *M* times stronger than that in systems using 2-D OVSF codes.

Figure 2-1 and 2-2 show the error probabilities versus the input energy per bit to noise power ratio, E_b/η_0 of the system using the three codes in an AWGN non-fading channel with 8 simultaneous users, and fixed number of carriers (*M*=8), and code length (*N*=32) and using by EGC and MRC reception methods, respectively. As shown in both figures, the performance of 2-D OVSF codes is always better than the 2-D random codes and 1-D Gold codes.

B. Error probability under a Rayleigh fading channel

In a Rayleigh fading channel, the orthogonality of 2-D OVSF codes would be destroyed due to the effects of phase change and amplitude fading, the performance of the systems with these three codes seemed almost the same no matter which codes are used. Figure 2-3 and 2-4 show error probabilities versus E_b/η_0 of the system using the three codes in a Rayleigh fading channel with 8 simultaneous users, *M*=8, and *N*=32 and using by EGC and MRC reception methods, respectively.

C. Error probability under a Rician fading channel

A Rician fading channel is associated with the AWGN non-fading channel and the Rayleigh fading channel. The relation between three channel models depends on the parameter *R*. For $R \to 0$, amplitude and phase tend to have well known Rayleigh distribution and uniform distribution, respectively. Whereas $R \to \infty$, they tend to have the same distribution in an AWGN non-fading channel model. Therefore, the fading effects when the received signal experiences in a Rician fading channel increase greatly as *R* decreases. Figure 2-5 and 2-6 show error probabilities versus E_b/η_0 of the system using the three codes in a Rician fading channel with 8 simultaneous users, *R*=10dB, *M*=8, and *N*= 32 and using by EGC and MRC reception methods, respectively.

2.5 Conclusions

In this project, a new 2-D OVSF codes, without the restrictions on the relationship of the number of frequency carriers and code lengths was proposed. They possess zero cyclic auto- and cross-correlation properties and can be used as both the channelization and scrambling codes. In other words, the two-layered spreading scheme used in W- CDMA is not necessarily needed with the new 2-D OVSF codes.

The multi-carrier system using our 2-D OVSF codes outperformed those using the 2-D random codes or 1-D Gold codes. Because of the orthogonality of the 2-D OVSF codes, the MAI caused by the specular terms could be eliminated and the interference can be significantly reduced.

But in a Rayleigh fading channel, code orthogonality would be destroyed and the proposed system would not gain any advantage as compared to those using 2-D random codes and 1-D Gold codes. Therefore, the performances of these codes seem almost the same no matter which codes are used.

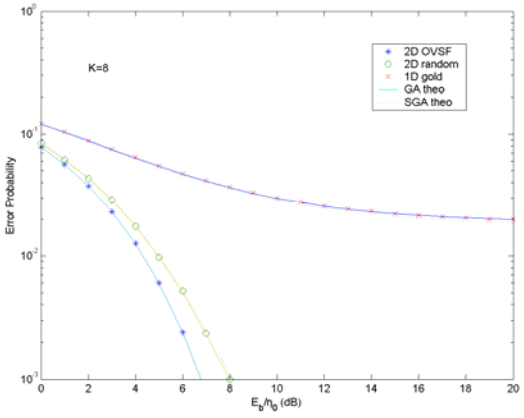

Figure 2-1: Error probability P_e versus E_b/η_0 for three codes in an AWGN channel with the EGC reception method.

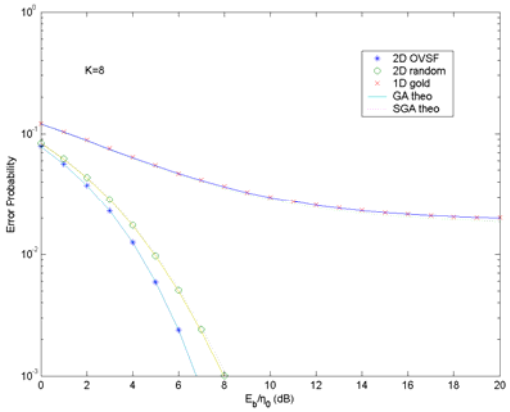

Figure 2-2: Error probability P_e versus E_b/η_0 for three codes in an AWGN channel with the MRC reception method.

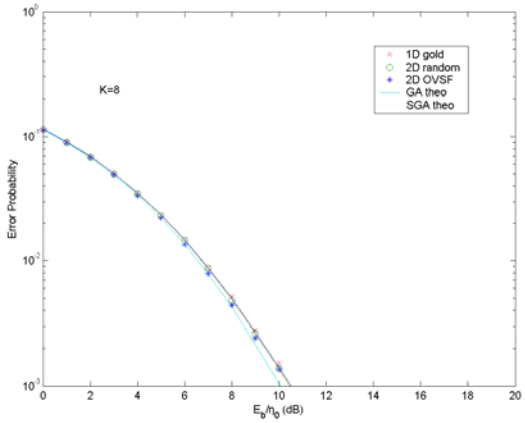

Figure 2-3: Error probability P_e versus E_b/η_0 for three codes in a Rayleigh fading channel with the EGC reception method.

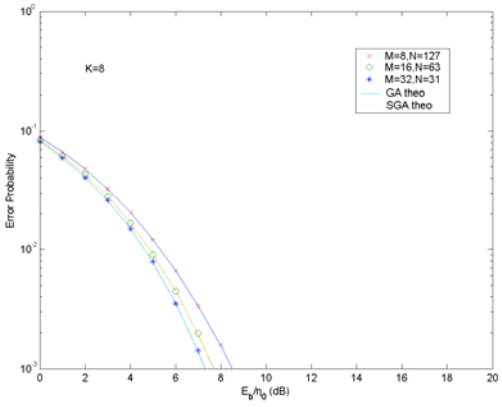

Figure 2-4: Error probability P_e versus E_b/η_0 for three codes in a Rayleigh fading channel with the MRC reception method.

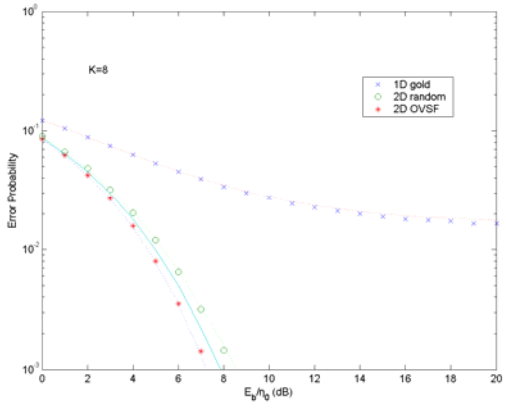

Figure 2-5: Error probability P_e versus E_b/η_0 for three codes in a Rician fading channel with R=10dB and EGC reception method.

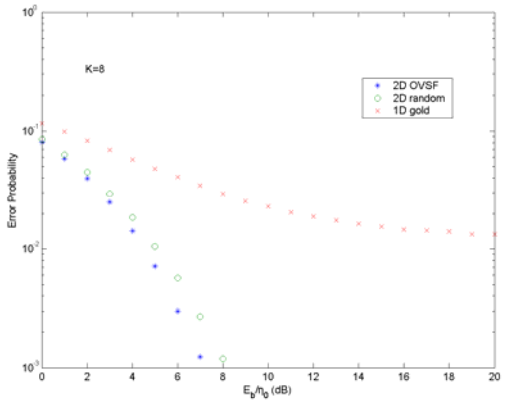

Figure 2-6: Error probability P_e versus E_b/η_0 for three codes in a Rician fading channel with R=10dB and the MRC reception method.

3. 下一世代無線行動接取技術-子計畫三：時空信號處理及多用戶檢測

3.1 Introduction

The Multiple-Input-Multiple-Output (MIMO) is an important technology to obtain higher data rate and to increase the system capacity compared with the conventional systems.

This sub-project proposes linear multiuser detectors (LMDs) and adaptive receivers for the synchronous direct sequence code division multiple access (DS/CDMA) systems under multipath fading. We propose robust LMDs in the multipath environment. We use the TLS algorithm [3.3] and ESPRIT algorithm [3.4][3.5] to develop the robust LMD and name it as the "TLS detector[3.6]" and "ESPRIT detector", respectively. Following, we propose several adaptive receiver structures to combat the drawback of slow convergence speed of the conventional LMS receivers. The ESPRIT algorithm can be employed to estimate the initial weight matrix and we name the method as the "ESPRIT-LMS receiver". Finally, we use LMS and ESPRIT-LMS algorithms to update the despreading sequence and obtain another new LMS receiver structure. We name this scheme as the "LMS sequence revising (LMS-SR) receiver" and "ESPRIT-LMS sequence revising (ESPRIT-LMS-SR) receiver".

3.2 System Model

We consider a synchronous DS/CDMA communication system with K active users under BPSK modulation. Each user is assigned a unique spreading sequence $\{c_k(t)\}_{k=1}^{K}$. The transmitted signal is given by

$$\mathbf{s}(t)=\sum_{k=1}^{K} b_k c_k(t), t\in[0,T_b] \qquad (3\text{-}1)$$

where b_k is the binary data bit transmitted by k-th user, T_b is the bit duration. The transmitter signal vector can be rewritten as

$$\mathbf{s}=\sum_{k=1}^{K}\mathbf{b}_k\mathbf{c}_k=\mathbf{C}\mathbf{b} \qquad (3\text{-}2)$$

where $\mathbf{s}$ is the transmitter signal vector, the dimension of $\mathbf{s}$ is equal to L at chip interval T_c, the antenna size of the transmitter is N. In the transmitter, we defined the transmitter signal, $\tilde{\mathbf{s}}(j)=[s((j-1)N+1)\ \ s((j-1)N+2)\ \ \ldots\ \ s((j-1)N+N)]^T$, $j=1,\ldots,J$ at interval NT_c. We consider a MIMO channel with N transmitted and M received antennas for a widely used discrete path physical model [3.1] can be written as

$$\mathbf{H}=\sum_{p=1}^{P}\mathbf{h}_p\mathbf{a}_R(\theta_{M,p})\mathbf{a}_T^H(\theta_{N,p})=\mathbf{A}_R(\theta_M)\mathbf{H}_p\mathbf{A}_T^H(\theta_N) \qquad (3\text{-}3)$$

where $\mathbf{H}$ is the channel matrix, $\mathbf{a}_T(\theta_N)$, $\mathbf{a}_R(\theta_M)$ are array steering by transmitter and receiver, respectively. The transmitter and receiver are coupled via P propagation paths with $\{\theta_{N,p}\}$ and $\{\theta_{M,p}\}$ as the spatial angles seen by the transmitter and receiver, respectively. The h_p represents the channel fading coefficient from p-th path. The received signal at the antenna array can be written as

$$\mathbf{x}(j)=\mathbf{H}\tilde{\mathbf{s}}(j)+\mathbf{n}(j),\ j=1,\ldots,J \qquad (3\text{-}4)$$

where $\mathbf{n}$ is a white Gaussian random vector. The array output signal $\mathbf{r}(j)$ is linearly combined through a complex weight matrix $\mathbf{W}$ to yield the array output signal that can be written as

$$\mathbf{r}(j)=\mathbf{W}^H\mathbf{x}(j),\ \mathrm{j}=1,\ldots,\mathrm{J} \qquad (3\text{-}5)$$

where $\mathbf{W}$ is weight matrix that can be ex-

pressed as $\mathbf{W} \in \{w_{mn}\}_{m=1,\ldots,M \ \mathrm{n}=1,\ldots,\mathrm{N}}$. From (3-4), we reconstitute the array output signal. Buffering the array output signal into blocks of length *J*, each block can be written in vector form

$$\tilde{\mathbf{r}} = \tilde{\mathbf{W}}^H \tilde{\mathbf{x}} \tag{3-6}$$

$$\tilde{\mathbf{x}} = [\mathbf{x}(1) \quad \mathbf{x}(2) \quad \cdots \quad \mathbf{x}(J)] = \tilde{\mathbf{H}}\mathbf{s} + \tilde{\mathbf{n}} = \tilde{\mathbf{H}}\mathbf{C}\mathbf{b} + \tilde{\mathbf{n}} \tag{3-7}$$

3.3 The Proposed Linear Multiuser Detectors

3.3.1 TLS Detector

We combine (3-6) and (3-7), the antenna array output signal can be written as

$$\tilde{\mathbf{r}} = (\mathbf{C} + \Delta\mathbf{C})\mathbf{b} + \tilde{\mathbf{W}}^H \tilde{\mathbf{n}} = (\mathbf{C} + \Delta\mathbf{C})\mathbf{b} + \mathbf{n}' \tag{3-8}$$

where ΔC denotes the perturbation of the spreading sequence. $\mathbf{n}'$ is also a white Gaussian noise matrix. For the TLS algorithm, ΔC and $\mathbf{n}'$ must satisfy

$$\begin{cases} \arg\min \left\| [\Delta\mathbf{C} \quad \mathbf{n}'] \right\| \\ \textit{subject to } (\mathbf{C} + \Delta\mathbf{C})\mathbf{b} + \mathbf{n}' = \tilde{\mathbf{r}} \end{cases}. \tag{3-9}$$

The TLS dictates the finding of a projection operator $\mathbf{P}_c$ of rank *k* subject to $\left\| [\Delta\mathbf{C} \quad \mathbf{n}'] \right\|_F^2 = \left\| [\mathbf{C} \quad \tilde{\mathbf{r}}] \right\|_F^2 - \left\| \mathbf{P}_c [\mathbf{C} \quad \tilde{\mathbf{r}}] \right\|_F^2$ is minimized.

From (3-9), assuming that the projection matrix $\mathbf{P}_c = \mathbf{E}_s \mathbf{E}_s^H$ where $\mathbf{E}_s^H \mathbf{E}_s = \mathbf{I}$, then

$$\left\| \mathbf{P}_c [\mathbf{C} \quad \tilde{\mathbf{r}}] \right\|_F^2 = tr\left(\mathbf{P}_c [\mathbf{C} \quad \tilde{\mathbf{r}}] [\mathbf{C} \quad \tilde{\mathbf{r}}]^H \mathbf{P}_c \right) = tr\left(\mathbf{E}_s^H \mathbf{C}\mathbf{C}^H \mathbf{E}_s \right). \tag{3-10}$$

The optimum $\mathbf{E}_s$ is composed of the *K* largest (nonzero) eigenvectors of the matrix $[\mathbf{C} \quad \tilde{\mathbf{r}}][\mathbf{C} \quad \tilde{\mathbf{r}}]^H$. The array output vector $\tilde{\mathbf{r}}$ is linearly transformed by a matrix **T** to attain an estimate on **b**. The TLS detector decision rule

$$\hat{\mathbf{b}}_{TLS} = \mathrm{sgn}\left(\mathbf{T}_{TLS}^T (\mathbf{C} + \Delta\mathbf{C})\mathbf{b}/L + \mathbf{T}_{TLS}^T \mathbf{n}'/L \right) \tag{3-11}$$

The particular hypothesis of the transmitting bit vector and each hypothesis is assumed equally likely with probability 2^{1-K}. The probability of error of the *k*-th user [3.7] is

$$P_{TLS,k} = 2^{1-K} \sum_{\mathbf{b} \in \{-1,1\}, b_k = -1} Q\left(\frac{-\sum_i \left(\mathbf{T}_{TLS}^T (\mathbf{C} + \Delta\mathbf{C})/L \right)_{ki} b_i}{\sigma \sqrt{\left(\mathbf{T}_{TLS}^T \mathbf{T}_{TLS} / L^2 \right)_{kk}}} \right) \tag{3-12}$$

3.3.2 ESPRIT Detector

The basic idea behind the ESPRIT algorithm is to exploit the so-called array displacement invariance structure. The channel matrix of the *i*-th sub array (i=1,2) as $\mathbf{H}_i$, then $\mathbf{H}_1 \equiv \mathbf{V}_{s1}\mathbf{H}$, $\mathbf{H}_2 \equiv \mathbf{V}_{s2}\mathbf{H}$. The ESPRIT algorithm exploits the shift invariance property of the array, which implies $\mathbf{H}_2 = \mathbf{H}_1 \mathbf{\Phi}$, $\mathbf{\Phi} = diag\left\{ e^{jk_c d \sin\theta_1}, \cdots, e^{jk_c d \sin\theta_P} \right\}$. Performing eigendecom- position on the input covariance matrix $\mathbf{R}_{\mathbf{xx}}$, we have $\mathbf{R}_{\mathbf{xx}} = \sum_{m=1}^{M} \boldsymbol{\lambda}_m \mathbf{u}_m \mathbf{u}_m^T$, $\{\lambda_m\}_{m=1}^M$, $\{\mathbf{u}_m\}_{m=1}^M$ are the eigenvalues and eigenvectors of $\mathbf{R}_{\mathbf{xx}}$, respectively. $\mathbf{u}_1, \mathbf{u}_2, \cdots, \mathbf{u}_{\mathrm{N}}$ are defined as signal eigenvectors, $\mathbf{u}_{N+1}, \mathbf{u}_{N+2}, \cdots, \mathbf{u}_{\mathrm{M}}$ are defined as noise eigenvectors. We have estimates for $\mathbf{U}_{s1}$ and $\mathbf{U}_{s2}$

$$\hat{\mathbf{U}}_{s1} = V_{s1} \hat{\mathbf{U}}_s \tag{3-13}$$

$$\hat{\mathbf{U}}_{s2} = V_{s2} \hat{\mathbf{U}}_s \tag{3-14}$$

$$\hat{\mathbf{U}}_{s1} = \hat{\mathbf{\Psi}} \hat{\mathbf{U}}_{s2} \tag{3-15},$$

where $\mathbf{U}_s = \mathbf{H}\mathbf{G}$ and $\mathbf{\Psi} = \mathbf{G}^{-1}\mathbf{\Phi}\mathbf{G}$.

From (3-15), we can employ the least squares to estimate **Ψ**. The least squares algorithm is

$$\hat{\mathbf{\Psi}}_{LS} = \arg\min \left\{ \left\| \hat{\mathbf{U}}_{s2} - \hat{\mathbf{U}}_{s1} \mathbf{\Psi} \right\|_F \right\} \tag{3-16}$$

$$= \left(\hat{\mathbf{U}}_{s1}^H \hat{\mathbf{U}}_{s1} \right)^{-1} \hat{\mathbf{U}}_{s1}^H \hat{\mathbf{U}}_{s2}. \tag{3-17}$$

The MIMO channel can be estimated as

$$\hat{\mathbf{H}} = \left[\hat{\mathbf{h}}_R(\hat{\theta}_1) \quad \hat{\mathbf{h}}_R(\hat{\theta}_2) \quad \cdots \quad \hat{\mathbf{h}}_R(\hat{\theta}_N) \right] \tag{3-18}$$

where the incident angle $\hat{\theta}_r = \sin^{-1}\left(\ln \hat{\lambda}_n \Big/ jk_c d \right)$, *n*=1,⋯ , *N* and $\hat{\mathbf{h}}_R(\hat{\theta}_r)$ is the array steering. From (3-8), if $\tilde{\mathbf{W}}^H \tilde{\mathbf{W}} = \mathbf{I}$, the data bit can be simply detected by despreader. The weight

matrix can thus be designed as $\tilde{\mathbf{W}}^H = \breve{\mathbf{H}}^+$, where $\mathbf{H}^+$ is the pseudoinverse of $\breve{\mathbf{H}}$. $\breve{\mathbf{H}} = diag\{\hat{\mathbf{H}} \ \hat{\mathbf{H}} \ \cdots \ \hat{\mathbf{H}}\}$. From (3-8), the ES-PRIT detector decision rule is

$$\hat{\mathbf{b}}_{ESP} = \mathrm{sgn}\left(\mathbf{T}_{ESP}^T \tilde{\mathbf{W}}^H \breve{\mathbf{H}} \mathbf{C}/L + \mathbf{T}_{ESP}^T \tilde{\mathbf{W}}^H \mathbf{n}'/L\right) \quad (3\text{-}19)$$

The probability of error of the *k*-th user is

$$P_{TLS,k} = 2^{1-K} \sum_{\substack{k \\ \mathbf{b}\in\{-1,1\}, b_k=-1}} Q\left(\frac{-\sum_i \left(\mathbf{T}_{TLS}^T (\mathbf{C}+\Delta\mathbf{C})/L\right)_{ki} b_i}{\sigma\sqrt{\left(\mathbf{T}_{TLS}^T \mathbf{T}_{TLS}/L^2\right)_{kk}}}\right) \quad (3\text{-}20)$$

3.4 Adaptive Receivers Based on LMD

3.4.1 LMS Receiver

We propose an adaptive LMD that is based on the LMS algorithm and the de-spreader output $\hat{\mathbf{b}}(n)$ can be written as

$$\hat{\mathbf{b}}(n) = \mathbf{C}^T \tilde{\mathbf{r}}(n)/L = \mathbf{C}^T \tilde{\mathbf{W}}^H(n)\tilde{\mathbf{x}}(n)/L \quad (3\text{-}21)$$

A linear receiver that comprising a weight matrix $\tilde{\mathbf{W}}$ operates on the input vector $\tilde{\mathbf{x}}$ to yield the output $\hat{\mathbf{b}}$. In a trained mode, the weight matrix $\tilde{\mathbf{W}}$ is chosen to minimize the cost function

$$J_{LMS} = E\left[\left\|\mathbf{C}^H \tilde{\mathbf{W}}^H(n)\tilde{\mathbf{x}}(n)/L - \mathbf{b}(n)\right\|^2\right] = E\left[\left\|\mathbf{e}(n)\right\|^2\right] \quad (3\text{-}22)$$

for LMS algorithm to derive the update equation of the weight matrix. The adaptive algorithm is as follows

$$\tilde{\mathbf{W}}(n+1) = \tilde{\mathbf{W}}(n) - \mu \frac{\partial J_{LMS}}{\partial \tilde{\mathbf{W}}} \quad (3\text{-}23)$$

$$= \tilde{\mathbf{W}}(n) - 2\mu\tilde{\mathbf{x}}(n)\mathbf{e}^H(n)\mathbf{C}^H/L \quad (3\text{-}24)$$

where μ is the step size. Next, we uses LMS algorithm to update despreading sequence. The elements of the despreading sequence are no longer ±1, it will be updated according to the sequence update equation. The sequence update equation is

$$\mathbf{C}(n+1) = \mathbf{C}(n) - \mu \frac{\partial J_{LMS}}{\partial \mathbf{C}}$$

$$= \mathbf{C}(n) - 2\mu\tilde{\mathbf{W}}^H(n)\tilde{\mathbf{x}}(n)\mathbf{e}^H(n)/L \quad (3\text{-}25)$$

3.4.2 ESPRIT algorithms Based LMS Receiver

In this section, we combine the ESPRIT algorithms and the LMS algorithms. From (3-24), the weight update equation of ES-PRIT-LMS algorithm can be modified as

$$\tilde{\mathbf{W}}(n+1) = \left(\breve{\mathbf{H}}^+\right)^H - 2\mu\tilde{\mathbf{x}}(n)\mathbf{e}^H(n)\mathbf{C}^H/L \quad (3\text{-}26)$$

the sequence update equation can be expressed as (3-25).

3.5 Simulation Results and conclusion

We use Walsh sequence with sequence length *L*=32. Compare the performance between the proposed receivers under the following MIMO DS/CDMA environments:

	Tx. ant.	Rx. ant.	User	Multipath
case 1	N=4	M=16	K=4	P=5
case 2	N=8	M=32	K=32	P=20

We compare the MSE learning curve and average uncoded bit error probability versus the average E_c/N_0 per bit of the proposed adaptive receiver under the environments case 1-2. The results are plotted in Figures 1-4 of report associated with sub-project 3. The simulation results show the convergence rate is as follows: ES-PRIT-LMS-SR > ESPRIT-LMS > LMS-SR > LMS. We also show the performance of the ESPRIT-based receivers is better than the TLS-based receivers (ESPRIT > TLS > ESPRIT-LMS-SR > ESPRIT-LMS > LMS-SR > LMS).

4. 下一世代無線行動接取技術-子計劃四：同步、通道估計與內接收機設計

4.1 Introduction

The main idea behind the orthogonal frequency division multiplexing (OFDM) waveform is to split a data block into multiple parallel sub-blocks so that each of them is transmitted by distinct orthogonal subcarriers. An OFDM-based system can overcome frequency selective fading in broadband wireless transmission and is the major reason for its current popularity.

With all its merits, OFDM, unfortunately, is far more sensitive to synchronization errors, especially the carrier frequency offset (CFO), than single carrier systems. CFO is primarily caused by relative movement or channel-induced Doppler shifts and instabilities of mismatch between transmitter and receiver oscillators [4.1]. Residual CFO results in inter-carrier interference (ICI) among subcarriers due to the loss of orthogonality and will bring about serious performance degradation. Whence, it is highly desirable to reduce the sensitivity of OFDM systems to CFO of any kind.

There have been a multitude of proposals for CFO compensation. But most of them require pilot symbols or training sequences [4.2], which lowers the effective data rate. We therefore face the dilemma of channel estimation in the presence of CFO and CFO estimation without pilots or reliable decisions. We adopt an iterative approach for joint CFO/channel estimation, tracking and data detection. To simply our problem, we shall assume that the initial CFO is to be less than one half of the subcarrier spacing. Drawing an analogy between the ICI effect on a frequency domain signal and the ISI effect on a time domain signal, we can easily apply the maximum likelihood sequence estimation (MLSE) technique to detect the data stream in the presence of ICI, assuming known CFO**.** Finally, we extend our investigation to a MIMO environment.

4.2 Joint CFO Estimation and Data Detection for SISO-OFDM

Assume that each OFDM symbol has a "useful interval" of length T_u and a cyclic prefix (CP) with duration T_g. In order to protect the OFDM signal against inter-symbol interference (ISI), the CP is set longer than the maximum channel memory, $T_g / T_u < 0.25$ being a practical value. The baseband signal is modulated by a Nyquist signaling pulse, up-converted to the radio frequency (RF) and then transmitted through the channel.

At the receiver, the signal is down-converted to the intermediate frequency (IF) and then demodulated. After removing the cyclic prefix, the signal part of the received time-domain baseband waveform can be expressed as

$$s[n] = \frac{1}{N}\sum_{k=0}^{N-1} a_k e^{j2\pi nk/N} e^{j2\pi f_e n/N} \tag{4-1}$$

where a_k represents the symbol carried by the *k*th subcarrier. The i.i.d data sequence $\{a_k\}$ is such that $E[a_k] = 0$ and $E[|a_k|^2] = 1$, N is the number of subcarriers, and f_e is CFO normalized by the intercar-

rier spacing $f_t = 1/T_u$ and T_u is an OFDM symbol period (without cyclic prefix).

This time domain signal is then passed through a serial-to-parallel converter and then an FFT demodulator. Assuming an AWGN channel, the signal at the FFT output becomes

$$r_k = \frac{1}{N}\sum_{n=0}^{N-1} s[n]w[n]e^{-j2\pi nk/N} + n_k \quad (4\text{-}2)$$

where $w[n]$ represents the receiver pulse shaping function and $n[k]$ is additive white Gaussian noise (AWGN). The received signal can be written as

$$\begin{aligned} r_k &= \sum_{m=0}^{N-1} a_m \left\{ \frac{1}{N}\sum_{n=0}^{N-1} w[n]e^{-j2\pi n(k-m)/N} e^{j2\pi f_e n/N} \right\} + n_k \\ &= \sum_m a_m W_{k-m}^{f_e} + n_k \\ &= a_k W_0^{f_e} + \underbrace{\sum_{m\neq k} a_m W_{k-m}^{f_e}}_{ICI} + n_k \\ &= y_k(f_e, \mathbf{a}) + n_k \end{aligned} \quad ,(4\text{-}3)$$

where

$$W_k^{f_e} = \frac{1}{N}\sum_{n=0}^{N-1} w[n]e^{-j2\pi nk/N} e^{j2\pi f_e n/N}.$$

As shown in (4-3), the signal portion of r_k, can be viewed as the output of an ISI channel driven by the input **a** with the channel response $W_k^{f_e}$, dependent upon the given CFO, f_e. The choice of the window function $w[n]$ affects the extent of ISI (actually the ICI in this case). To control the complexity of the estimator, the length of $W_k^{f_e}$ must be kept reasonably short.

(i) Data detection:

With a proper window shaping, we can rewrite (4-3) as

$$r_k \approx a_k W_0^{f_e} + \sum_{m=k-L, m\neq k}^{m=k+L} a_m W_{k-m}^{f_e} + n_k \quad (4\text{-}4)$$

where L is usually less or equal than 2 for $|f_e| < 0.5$.

Given $\hat{f}_e$, the data detection is equivalent to estimating the state of a discrete-time finite-state machine. The finite-state machine in this case is the equivalent discrete-time channel with coefficients $\{W_k^{\hat{f}_e}\}$ and its state at any instant is given by the *2L* most recent inputs. Even though we have non-causal term in (4-4), we can add a delay function so that the resulting model is causal.

$$r_{K-L} \approx a_k W_{-L}^{\hat{f}_e} + a_{k-1} W_{-L+1}^{\hat{f}_e} + \cdots + a_{k-2L} W_L^{\hat{f}_e} + n_{k-L} \quad (4\text{-}5)$$

The state at time *k* is

$$S_k = (a_{k-1}, a_{k-2}, \cdots, a_{k-2L}) \quad (4\text{-}6)$$

If the information symbols are *M*-ary, the channel filter has M^{2L} states. Consequently, the channel is described by an M^{2L}-state trellis and the Viterbi algorithm may be used to determine the most probable path through the trellis.

(ii) CFO estimation:

Given $\hat{a}$ as well as **r**, we can get a CFO estimate by finding f_e that minimizes the cost function

$$C(f_e) = \sum_k |r_k - y_k(f_e, \hat{\mathbf{a}})|^2 \quad (4\text{-}7)$$

The minimization of (4-7) is carried out base on a gradient descent search method as following:

$$\begin{aligned} \nabla_{f_e}(C(f_e)) &= \frac{\partial C}{\partial f_e} \\ &= \sum_k \left\{ -A \cdot r_k^* - A^* r_k + BA^* + AB^* \right\} \end{aligned} \quad (4\text{-}8)$$

where $()^*$ denotes the complex conjugate and

$$A = \sum_m a_m \left(W_{k-m}^{f_e}\right)' \approx \sum_{m=k-L}^{k+L} a_m \left(W_{k-m}^{f_e}\right)'$$
$$B = \sum_m a_m \left(W_{k-m}^{f_e}\right) \approx \sum_{m=k-L}^{k+L} a_m \left(W_{k-m}^{f_e}\right) \quad (4\text{-}9)$$
$$\left(W_{k-m}^{f_e}\right)' = \frac{\partial W_{k-m}^{f_e}}{\partial f_e}$$

A *learning rate u* is introduced to control the rate of change in each iteration

$$\begin{aligned} f_e^1 &\leftarrow f_e^0 - u * \nabla_{f_e}(C(f_e^0)) \\ f_e^2 &\leftarrow f_e^1 - u * \nabla_{f_e}(C(f_e^1)) \\ &\vdots \\ f_e^m &\leftarrow f_e^{m-1} - u * \nabla_{f_e}(C(f_e^{m-1})) \end{aligned}$$

When f_e^m reaches a stable value with very little jitter, which indicates that we have arrived at a minimum, the algorithm stops.

The joint frequency-data sequence (FD) estimation algorithm consists of the following steps:

A.1 (Frequency Estimate Initialization) Set the initial estimate $\hat{f}_e$ to zero.

A.2 (Starting the FD iteration loop) Using the CFO estimate $\hat{f}_e$, generate the corresponding frequency domain "channel response" $W_k^{f_e}$:

$$W_k^{f_e} = \frac{1}{K}\sum_{n=0}^{K-1} w[n] e^{-j2\pi m(k-m)} e^{j2\pi f_e n/K}$$

A.3 (Compute the tentative data estimate) Based on the observation baseband samples *r*, we run the Viterbi algorithm using the branch metric

$$\lambda_k = \left| r_k - y_k\left(\hat{f}_e, a\right)\right|^2$$

to obtain an estimate $\hat{a}$ of the transmitted data sequence.

A.4 (Update the frequency estimate) Given $\hat{a}$ from Step 3 as well as **r**, we obtain a new CFO estimate by searching for f_e that minimizes the cost function

$$C = \sum_k \left| r_k - y_k\left(f_e, \hat{a}\right)\right|^2$$

A.5 (Convergence check and end of the FD loop) If the new CFO estimate is close enough to the previous estimate, i.e. absolute difference is less than 10^{-6}, then stop the iteration and release the most recent estimate; otherwise, go to Step 2. Simulation shows that this algorithm usually converges within just two or three iterations.

4.3 Joint Estimation for Frequency-Selective Channels

(i) System model for frequency-selective channels

For frequency-selective fading channels, we assume that the CP is longer than the channel impulse response whence there is no frequency domain self interference between successive OFDM symbols. With such an assumption we can concentrate on a single OFDM symbol scenario. Let the signal part of the received signal be given by

$$s[n] = \frac{1}{N}\sum_{k=0}^{N-1} a_k H_k e^{j2\pi nk/N} e^{j2\pi f_e n/N} \quad (4\text{-}10)$$

where H_k is the channel response at *k/T*. After taking FFT, the received signal becomes

$$\begin{aligned} r_k &= \sum_{m=0}^{N-1} a_m H_m W_{k-m}^{f_e} + n_k \\ &= y_k(f_e, \mathbf{a}, \mathbf{H}) + n_k \end{aligned} \quad (4\text{-}11)$$

(ii) Joint frequency-data sequence-channel (FDC) estimation algorithm

The estimator proposed in the previous section cannot be applied directly to (4-11) because the channel response is unknown. However, assuming the data sequence and the CFO are known, the channel impulse response can be easily estimated.

For every subcarrier *n*, the channel can be estimated by using least squared method. Based on this channel estimator and the joint CFO-data sequence estimator proposed in the previous section, we arrive at the following iterative joint CFO-data sequence-channel estimation algorithm.

B.1 (Channel estimate initialization) Let $\hat{H}_o$ to be the channel estimate from the previous OFDM symbol interval.

B.2 (FD iteration loop) Using this channel estimate, the CFO f_e and the symbol sequence **a** are estimated by the joint FD estimation algorithm described in the previous section.

B.3 (Channel estimate update) Compute a new channel estimate $\hat{H}_N$ using least squared method based on the current estimates $\hat{f}_e$ and $\hat{a}$.

B.4 (Convergence check for the channel estimate) If the new channel estimate $\hat{H}_N$ is close enough to the previous estimate, more specifically, if $\left|\frac{\hat{H}_N - \hat{H}_o}{\hat{H}_N}\right|^2 < 10^{-2}$ then stop iteration and release the most recent estimates. If not, go to Step 2.

(iii) Numerical Experiments

The computer simulation results reported in this section are obtained by using a pilot and data format, which are the same as the Tgn Sync 802.11n proposal (52 data tones and 4 pilot tones). It is a slight modification of the IEEE 802.11a data format (48 data tones and 4 pilot tones).

From Fig. 6 in report of sub-project 4, we can see that the proposed joint FD estimator gives good BER performance in AWGN channels. The frequency-selective fading channel is modelled as an linear FIR filter with impulse response given by

$$h(k) = \sum_{n=0}^{C_L-1} \alpha_n e^{-j\Phi} \delta(k-n) \quad (4\text{-}12)$$

where Φ is uniformly distributed in $(0,2\pi]$ and α_n is Rayleigh distributed with an exponential power profile

$$\overline{\alpha_n^2} = (1 - e^{-T_s/T_{rms}}) e^{-nT_s/T_{rms}}$$

with C_L=10, T_{rms}=30ns and T_s=50ns. We use Jakes channel model with maximum Doppler shift of 500 Hz to simulate time-correlated Rayleigh fading α_n.

As shown in report of sub-project 4, the performance curves indicate that the BER performance is dominated by the channel estimation error since the MSEE of the CFO estimator is relatively small, especially at high SNRs where the MSEE of our frequency estimate reaches an almost constant floor

while the channel estimate's MSEE continues to decrease.

4.4 Joint Estimation for MIMO-OFDM Systems

(i) System Model

Consider a MIMO system with M_T transmit antennas and M_R receive antennas. Assuming a flat block-fading channel model, we can express the equivalent signal part of the received time-domain samples at qth receive antenna as

$$b^q[n] = \sum_{p=1}^{M_T} \tilde{s}^{p,q}[n], q = 1,2,\cdots,M_R \qquad (4\text{-}13)$$

where

$$\tilde{s}^{p,q}[n] = \frac{1}{N}\sum_{k=0}^{N-1}\sqrt{\frac{E_s}{M_T}}a_k^p H_k^{q,p} e^{j2\pi mk/N} e^{j2\pi f_e n/N} \qquad (4\text{-}14)$$

corresponds to the OFDM signal sent from the pth transmit antenna to the qth receive antenna, where a_k^p represents the symbol carried by the kth subcarrier at the pth transmit antenna, $H_k^{q,p}$ is the kth subcarrier's channel transfer function between the qth receive antenna and the pth transmit antenna, E_s is the average energy allocated to the kth subcarrier across the transmit antennas, f_e **i**s the CFO normalized by the inter-carrier spacing, and N is the total number of sub-carriers for each transmit antenna.

After establishing proper frame (symbol) timing, removing the cyclic prefix and taking FFT on the time-domain samples, the received baseband frequency domain signal at the qth RX antenna reads

$$\begin{aligned} r_k^q &= \sum_{n=0}^{N-1}\tilde{b}^q[n]e^{-j2\pi nk/N} + n_k^q \\ &= \sum_{p=1}^{M_T}\sum_{m=0}^{N-1} a_m^p H_m^{q,p} W_{k-m_e}^{f_e} + n_k^q \\ &= \sum_{p=1}^{M_T} y_k\left(f_e, a^p, H^{q,p}\right) + n_k^q, q = 1,2,\cdots,M_R \end{aligned} \qquad (4\text{-}15)$$

where $\tilde{b}^q[n]$ is the "folding window signal" from all transmit antennas.

Comparing the above equation with (4-11), we find that to apply the joint FDC method to solve (4-15), we will have a trellis with the number of trellis states equals to M^{2L*M_T} since we now have to consider all transmitted data streams from all transmit antennas.

(ii) MIMO-OFDM Channel Estimation

Rewriting (4-15) in matrix form (for qth RX antenna)

$$\begin{bmatrix} r_0^q \\ r_0^q \\ \vdots \\ r_{N-1}^q \end{bmatrix} = \begin{bmatrix} W_0^{f_e} & \cdots & W_{-N+1}^{f_e} \\ \vdots & \ddots & \vdots \\ W_{N-1}^{f_e} & \cdots & W_0^{f_e} \end{bmatrix} \begin{bmatrix} \sum_{p=1}^{M_T} H_0^{q,p} a_0^p \\ \sum_{p=1}^{M_T} H_1^{q,p} a_1^p \\ \vdots \\ \sum_{p=1}^{M_T} H_{N-1}^{q,p} a_{N-1}^p \end{bmatrix} + \begin{bmatrix} n_0^q \\ n_1^q \\ \vdots \\ n_{N-1}^q \end{bmatrix} \qquad (4\text{-}16)$$

and invoking the substitutions,

$$\mathbf{r}^q = \begin{bmatrix} r_0^q & r_0^q & \cdots & r_{N-1}^q \end{bmatrix}^T,$$

$$\mathbf{n} = \begin{bmatrix} n_0^q & n_0^q & \cdots & n_{N-1}^q \end{bmatrix}^T,$$

$$\mathbf{H_A^q} = \begin{bmatrix} \left(H_A^q\right)_0 & \left(H_A^q\right)_1 & \cdots & \left(H_A^q\right)_{N-1} \end{bmatrix}^T = \begin{bmatrix} \sum_{p=1}^{M_T} H_0^{q,p} a_0^p & \sum_{p=1}^{M_T} H_1^{q,p} a_1^p & \cdots & \sum_{p=1}^{M_T} H_{N-1}^{q,p} a_{N-1}^p \end{bmatrix}^T,$$

$$\textbf{and} \quad \mathbf{F} = \begin{bmatrix} W_0^{f_e} & \cdots & W_{-N+1}^{f_e} \\ \vdots & \ddots & \vdots \\ W_{N-1}^{f_e} & \cdots & W_0^{f_e} \end{bmatrix},$$

we obtain

$$\mathbf{r^q} = \mathbf{F}\mathbf{H}_\mathbf{A}^\mathbf{q} + \mathbf{n} \quad (4\text{-}17)$$

Assuming the data sequence and the CFO are known, we first compensate for the CFO through the LS estimate

$$\mathbf{H}_\mathbf{A}^\mathbf{q} = \left[\left(\hat{H}_A^q\right)_0 \quad \left(\hat{H}_A^q\right)_1 \quad \cdots \quad \left(\hat{H}_A^q\right)_{N-1}\right]^T \quad (4\text{-}18)$$
$$= (\mathbf{F}^\mathbf{H}\mathbf{F})^{-1}\mathbf{F}^\mathbf{H}\mathbf{r}^\mathbf{q}$$

The kth subcarrier over M_R receive antennas reads

$$\left(\hat{\mathbf{H}}_A\right)_{k,t} = \left[\left(\hat{\mathbf{H}}_A^1\right)_{k,t} \quad \left(\hat{\mathbf{H}}_A^2\right)_{k,t} \quad \cdots \quad \left(\hat{\mathbf{H}}_A^{M_R}\right)_{k,t}\right]^T$$

$$\mathbf{A_{k,t}} = \left[a_{k,t}^1 \quad a_{k,t}^2 \quad \cdots \quad a_{k,t}^{M_T}\right]^T$$

where the index $1 \le t \le M$ denotes the tth OFDM symbol of an M-symbol block that suffer from the same flat (block-)fading.

Finally, the channel matrix can be estimated by

$$\widehat{\mathbf{H}}_k = \overline{(\widehat{\mathbf{H}}_A)}_k \ \overline{\mathbf{A}}_k^H (\overline{\mathbf{A}}_k \overline{\mathbf{A}}_k^H)^{-1} \quad (4\text{-}19)$$

where

$$\overline{(\widehat{\mathbf{H}}_A)}_k = [(\widehat{\mathbf{H}}_A)_{k,1} \ (\widehat{\mathbf{H}}_A)_{k,2} \ \cdots \ (\widehat{\mathbf{H}}_A)_{k,M}]$$
$$\overline{\mathbf{A}}_k = [\mathbf{A}_{k,1}, \mathbf{A}_{k,2}, \cdots, \mathbf{A}_{k,M}]$$

$\hat{\mathbf{H}}_k$ is the M_RxM_T complex channel matrix for the kth subcarrier on the premise that the rank of $\overline{\mathbf{A}}_k$, the "over symbols data matrix at subcarrier k" is greater than M_T. In other words, one has to sent at least M_T OFDM symbols over the same flat fading block (a coherent time) in order to obtain a proper channel estimate .

(iii) An Iterative Joint FDC Estimation Algorithm

Based on the above discussion, we suggest an iterative joint FDC estimation algorithm as follows.

C.1 (Channel estimate initialization) Set $\hat{H}_o$ to be the channel estimate from the previous OFDM symbols.

C.2 (Frequency Estimate Initialization) Set the initial estimate $\hat{f}_e = 0$.

C.3 (Starting the FD iteration loop) Use current channel estimate for the frequency-data sequence iteration loop. Calculate the channel frequency response compensation matrix $F = \left[W_k^{f_e}\right]$ and current frequency estimate $\hat{f}_e$.

C.4 (Compute the tentative data estimate) Given the observed sample vector **r**, perform the Viterbi algorithm with the branch metric

$$\lambda_k^q = \left| r_k^q - \sum_{p=1}^{MT} y_k\left(\hat{f}_e, a^p, \hat{H}^{p,q}\right)\right|^2$$

to find a conditional optimal data sequence estimate $\hat{a}$.

C.5 (Update the frequency estimate) Update the CFO estimate by minimizing the cost function:

$$C = \sum_q \sum_k \left| r_k^q - \sum_{p=1}^{MT} y_k\left(\hat{f}_e, a^p, \hat{H}^{p,q}\right)\right|^2$$

C.6 (Convergence check and end of the FD loop) If the new CFO estimate $\hat{f}_e$ is close to the previous estimate, i.e. absolute difference is less than 10^{-6}, then stop the current FD iteration and release the new estimates

$\hat{a}$ and $\hat{f}_e$; otherwise go back to Step 3.

C.7 (Channel estimate update) Compute a new channel estimate $\hat{H}_N$ using (4-19) based on the current estimates $\hat{a}$ and $\hat{f}_e$.

C.8 (Convergence check for the channel estimate) If the new channel estimate $\hat{H}_N$ is close enough to the previous estimate, more specifically, if

$$\left| \frac{\hat{H}_N - \hat{H}_o}{\hat{H}_N} \right|^2 < 10^{-2}$$

then stop iteration and release the most recent estimates. Otherwise, go to Step 3.

(iv) Numerical Experiments

From the simulation results, we observe that the spatial diversity does pay off--with a gain of more than 4 dB for BER<10^{-2}. Similarly, we find that more receive antennas leads to better performance due to the MIMO diversity gain. Also, the model-based channel estimation still outperform the LS channel estimate for MIMO-OFDM systems.

4.5 Conclusion

We have presented iterative joint estimation and detection algorithms for OFDM systems in various scenarios. An iterative joint frequency estimation and data sequence detection algorithm is first given for AWGN channels. By incorporating a proper channel estimation method, we then provide an iterative joint FDC estimation algorithm for SISO-OFDM systems. Some refinements for enhanced performance and complexity reduction are suggested. Finally, we extend our joint FDC estimation algorithm to MIMO-OFDM environments. Simulation based on a candidate IEEE 802.11n standard--the Tgn Sync (Task Group *n*) [4.10] proposal--is provided to validate various joint estimation and detection algorithms. The corresponding numerical results do prove that the proposed solutions are both practical under the assumed channel conditions. Our solution can operate in the blind mode if the initial CFO is less than half of a subcarrier spacing. Otherwise, we can use the preamble (like the 802.11n case) to reduce the CFO to within the desired range. Our proposal can then be used for subsequent data detection and CFO/channel tracking in time-varying channels.

5. Reference

[1.1] N. Yee and J.-P. Linnartz, "Controlled equalization of multi-carrier CDMA in an indoor Rician fading channel," *Proc. of IEEE VTC'94,* Jan. 1994, vol. 3, pp. 1665-1669.

[1.2] A. Clouly, A. Brajal and S. Jourdan, "Orthogonal multicarrier techniques applied to direct sequence spread spectrum CDMA system," *Proc. of IEEE GLOBECOM'93,* Nov. 1993, pp. 1723-1728.

[1.3] E. Sourour and M. Nakagawa, "Performance of orthogonal MC CDMA in a multipath fading channel," *IEEE Trans. Veh. Tech.,* vol. 44, no. 3, pp. 356-367, Mar. 1996.

[1.4] S. Hara and R. Prased, "Overview of multicarrier CDMA," *IEEE Commun. Mag.,* vol. 35, no. 12, pp. 126-133, Dec. 1997.

[1.5] S. Kondo and L. B. Milstein, "Performance of multicarrier DS CDMA

systems," *IEEE Trans. Commun.,* vol. 44, no. 2, pp. 238-246, Feb. 1991.

[1.6] S. M. Tseng and M. R. Bell, "Asynchronous multicarrier DS- CDMA using mutually orthogonal complementary sets of sequences," *IEEE Trans. Commun.,* vol. 48, no. 1, pp. 53-59, Jan. 2000.

[1.7] F. Adachi, M. Sawahashi and K. Okawa, "Tree-structured generation of orthogonal spreading codes with different length for forward link of DS-CDMA mobile radio," *Elect. Lett.,* vol. 33, no. 1, pp. 27-28, Jan. 1997.

[1.8] E. H. Dinan and B. Jabbari, "Spreading codes for direct sequence CDMA and wideband CDMA cellular networks," *IEEE Commun. Mag.,* vol. 36, no. 9, pp.48-54, Sept. 1998.

[1.9] C.-M. Yang, G.-C. Yang, P.-H. Lin and W.C. Kwong, "2-D orthogonal spreading codes for multi-carrier DS-CDMA systems," *ICC'03, IEEE International Conference on*, vol. 5, pp. 3277-3281, May 2003.

[3.1] A. M. Sayeed, "Deconstructing Multi-Antenna Fading Channels," IEEE Trans. on Signal Processing (special issue on MIMO systems), pp. 2563-2579, Oct. 2002.

[3.2] H. Liu and G. Xu, "A subspace method for signature waveform estimation in synchronous CDMA systems," IEEE Trans. Commun., vol. COM-44, No.10, pp. 1346-1354, Oct. 1996.

[3.3] G.H. Golub and C.F. Van Loan, Matrix Computations, 2nd ed., Johns Hopkins university Press 1989.

[3.4] R. Roy. ESPRIT: Estimation of Signal Parameters via Rotational Invariance Techniques. Ph.D. Dissertation, Stanford University, Stanford, California, 1987.

[3.5] B. D. Rao and K. V. S. Hari, "Performance analysis of ESPRIT and TAM in determining the direction of arrival of plane waves in noise," IEEE Trans. Acoust., Speech, Signal Process., vol.ASSP-37, pp. 1990-1995, December 1989.

[3.6] Wei-Chiang Wu and Shang-Chun Tsai, "A TLS-based Linear Multiuser detector for Synchronous DS/CDMA Communication System," COM-1-3, Proceeding of the 2002 National Symposium on Telecommunications.

[3.7] W.C. Wu and J.W.Dai, "Adaptive Detection for Synchronous CDMA Multipath Signal Based on Signature Waveform Tracking," IEICE Transaction on Fundamentals of Electronics, Communications and Computer Sciences, vol. E84-A, no.12, pp. 3077-3081, Dec. 2001.

[4.1] T. Pollet, M. Van Bladel, and M. Moeneclaey, `"BER sensitivity of OFDM systems to carrier frequency offset and Wiener phase noise," *IEEE Trans. Commun*., vol. 43, pp. 191 - 193, Feb./Mar./Apr. 1995.

[4.2] P.-H. Moose, "A technique for orthogonal frequency-division multiplexing frequency offset correction," *IEEE. Trans. Commun.*, vol. 42, pp. 2908-2914, Oct. 1994.

[4.3] H. Bolcskei, "Blind estimation of symbol timing and carrierfrequency offset in wireless OFDM systems," *IEEE Trans. Commun.*, vol. 49, pp. 988-999, June 2001.

[4.4] M. Biguesh and A. B. Gershman,"MIMO channel estimation: optimal training and tradeoffs between estimation techniques," *2004 IEEE Intern. Conf. on Commun.* vol. 5, pp. 2658-2662, June 2004.

[4.5] G. J. Foschini and M. J. Gans, "On limits of wireless communications in a fading environment when using multiple antennas," *Wireless Personal Communications*, pp. 311-335, 1998.

[4.6] E. Telatar, "Capacity of multi-antenna Gaussian channels," *European Trans. on Telecommunications*, vol. 10, pp. 585-596, 1999.

[4.7] G. D. Golden, C. J. Foschini, and P. W. Wolniansky, “Detection algorithm and initial laboratory results using V-BLAST space-time communication architecture,” *Electronics Letters,* vol. 35, pp. 14-16, 1999.

[4.8] M. X. Chang and Y. T. Su, “Model-based channel estimation for OFDM signals in Rayleigh fading,” *IEEE Trans. Commun*., vol. 50, pp. 540-544, Apr. 2002..

[4.9] Y. Zhao and A. Huang, “A novel channel estimation method for OFDM communization systems based on pilot signals and transform-domain processing,” in *Proc. IEEE 47th Vech. Tech. Conf.*, Phoenix, USA, pp. 2089-2093, May 1997.

[4.10] “TGn Sync proposal technical specification,"” TGn Sync, Aug. 2004.